Catalysis Science & Technology

PAPER

View Article Online
View Journal

Cite this: DOI: 10.1039/c7cy02339a

Direct *versus* acetalization routes in the reaction network of catalytic HMF etherification†

P. Lanzafame, *[a] G. Papanikolaou,[a] S. Perathoner,[a] G. Centi, [a] M. Migliori, *[b] E. Catizzone,[b] A. Aloise[b] and G. Giordano[b]

The etherification of HMF (5-hydroxymethylfurfural) to EMF (5-(ethoxymethyl)furan-2-carbaldehyde) is studied over a series of MFI-type zeolite catalysts containing different heteroatoms (B, Fe, Al), aiming to understand the effect of different isomorph substitutions in the MFI framework on the reaction pathways of HMF conversion. The rate constants in the reaction network are determined for these different catalysts and analyzed with respect to the amount of Brønsted and Lewis acid sites determined by FT-IR pyridine adsorption. Two different pathways of EMF formation, *i.e.* direct etherification and *via* acetalization, were evidenced. The Lewis acid sites generated from the presence of aluminum are primarily active in catalyzing direct HMF etherification to EMF, which has a rate constant about one order of magnitude lower than the etherification of the corresponding acetals. This behaviour is due to the competitive chemisorption between hydroxyl and aldehyde groups (both present in HMF) on the Lewis acid sites catalyzing the etherification. A cooperation phenomenon between Brønsted and Lewis acid sites is observed for the HMF acetal etherification to EMF acetal. In the reactions of direct HMF acetalization and deacetalization of the EMF acetal, the turnover frequencies for Silicalite-1 and B-MFI samples are about twice those for Fe-MFI and Al-MFI samples. This is attributed to the different reactivity of strong silanol groups associated with surface defects on the external surface in Silicalite-1 and B-MFI. These sites are also responsible for the EMF-to-EOP (ethyl 4-oxopentanoate) reaction step. In the deacetalization reaction of the EMF acetal, the behavior is determined from the presence of water (product of reaction) favouring the back reaction (aldehyde formation).

Received 16th November 2017,
Accepted 29th January 2018

DOI: 10.1039/c7cy02339a

rsc.li/catalysis

Introduction

Etherification is a relevant reaction in the liquid phase transformation of biomass platform molecules,[1,2] for example to produce i) diesel additives by etherification of furanyl alcohol[3] or HMF (5-hydroxymethylfurfural),[4–6] ii) mono-alkylated products used to obtain high quality alkyl naphthenic kerosene by HMF self-etherification[7] to 5,5′-oxy(bismethylene)-2-furaldehyde (OBMF), which is an interesting prepolymer and antiviral precursor,[8] and 5-alkoxymethylfuroate for a new class of biodegradable anionic surfactants by HMF selective etherification.[9] Other relevant etherification reactions include glycerol etherification with isobutene,[10,11] methanol etherification to DME,[12–14] and methyl *tert*-butyl ether (MTBE) synthesis from methanol and isobutene.[15] In general, it is known that both Brønsted and Lewis acid sites could be active in these reactions and that it is necessary to tune the acidity because of the presence of other reactions, such as acetalization, competing with etherification in HMF conversion, although it may also lead to interesting products (biodegradable surfactants).[16] In fact, different types of functional groups (alcoholic, aldehydic) are present in HMF as well as in other platform molecules, and the control of catalyst reactivity is thus a relevant aspect from the application perspective.[17]

Although oxide-,[4a,6] carbon-[18] and ion-exchange resin-type[3] catalysts have been used for HMF etherification, zeolite-type catalysts[4b,19,20] offer the advantage of fine tuning the acidity features (amount, nature and strength of the Brønsted and Lewis sites),[20c] allowing better understanding of the role of these active sites in the reaction network of HMF etherification, including the possible presence of cooperative effects. In fact, recently, the presence of cooperative effects between Lewis and Brønsted acid sites has been reported in glucose transformation over zeolites,[21] H-transfer in furfural conversion,[22] multistep biomass conversion[23] and glycerol dehydration.[24]

[a] *Departments of ChiBioFarAm and MIFT- Section of Industrial Chemistry, University of Messina, ERIC aisbl and CASPE-INSTM, V.le F. Stagno d'Alcontres 31, 98166 Messina, Italy. E-mail: planzafame@unime.it*
[b] *Department of Environmental and Chemical Engineering, University of Calabria, via Bucci, 87036 Rende, Italy. E-mail: massimo.migliori@unical.it*

† Electronic supplementary information (ESI) available. See DOI: 10.1039/c7cy02339a

The aim of this paper is to analyze how the rate constants in the reaction network of HMF etherification with ethanol depend on the nature and amount of the Lewis and Brønsted acid sites, which are changed in a homogenous series of MFI-type zeolites containing different heteroatoms, T-Silicalite-1 (T = B, Fe and Al). The analysis of the results provides some novel insight into the role of these acid sites in the different steps of the reaction network of HMF etherification and the presence of cooperative effects, leading to different reaction pathways over different catalysts.

Results and discussion

Characterization of the catalysts

The XRD patterns of the synthesized samples (Fig. 1a) show characteristic peaks of the MFI-type topology without any evidence of the presence of other phases.[25] The comparison of the XRD patterns in the 2θ range from 20 to 28°, reported in Fig. 1b, reveals the presence of a doublet reflection around 2θ = 25° for Silicalite-1 and Al-MFI, which is characteristic of a monoclinic symmetry. For B-MFI, a single reflection at 2θ = 24.4° ascribed to orthorhombic symmetry is observed, while both framework symmetries are present for the Fe-MFI sample.[26]

The results of scanning electron microscopy (SEM) for all prepared samples are shown in Fig. 2. For Silicalite-1, a round-like shape morphology for crystals with a relatively uniform size of 2 μm is observed.[4b] The intergrowth of smaller crystals with a typical coffin-shape was also observed for this sample. Crystals with different sizes and morphologies were observed for the other samples. The image in Fig. 2b indicates that B-MFI consists of heavily twinned near-spherical crystals with a size of about 10 μm. The incorporation of iron in the MFI-type structure led to a more jagged morphology of elliptical crystallites with a size of about 5 μm (Fig. 2c). Furthermore, the SEM images confirmed that the preparation of the Al-MFI sample produced more elongated crystals, which present a non-homogeneous dimension (Fig. 2d).

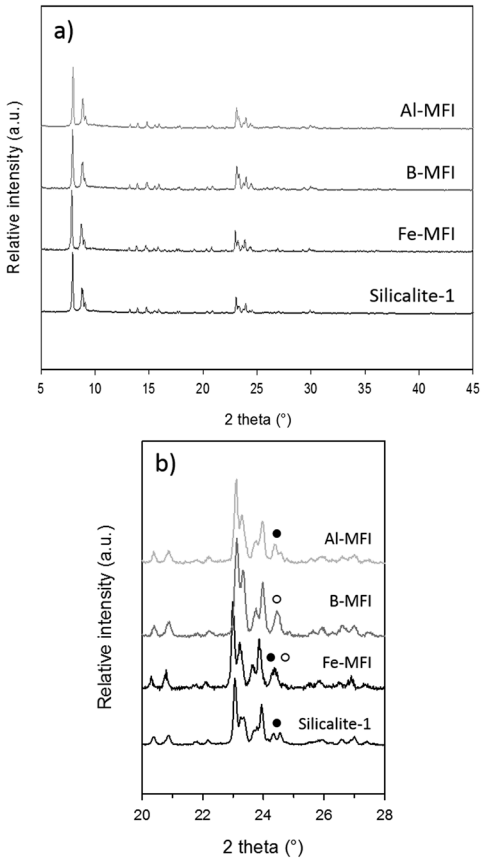

Fig. 1 X-ray diffractograms of MFI-type catalysts in the 2θ ranges 5–45° (a) and 20–28° (b).

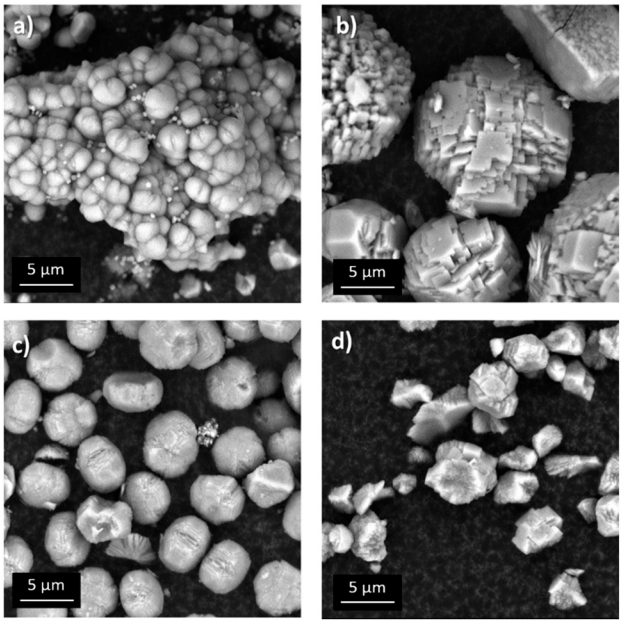

Fig. 2 SEM images of the samples: Silicalite-1 (a), B-MFI (b), Fe-MFI (c) and Al-MFI (d).

The textural characteristics of the investigated catalysts were determined by nitrogen adsorption measurement (Table 1). All samples exhibit high BET surface areas (366–408 $m^2\ g^{-1}$) and micropore volumes (0.079–0.110 $cm^3\ g^{-1}$) in the typical range of an MFI structure,[27–29] in accord with their good XRD crystallinity (Fig. 1a). Furthermore, a marked reduction in the external surface area was observed for T-Silicalite-1 containing heteroatoms.

The acidity of the catalysts was studied by NH_3-TPD and pyridine FT-IR measurements. The profiles of NH_3-TPD (see Fig. S1 in the ESI†) can be deconvoluted into two peaks related to weak and medium–strong acid sites, in the temperature range of 100–300 °C and 300–450 °C, respectively. The total acidity decreases following the order Al-MFI > Fe-MFI > B-MFI > Silicalite-1. After the introduction of the heteroatoms, a different distribution in the strength of acid sites was also observed. From the ratio of the two deconvolution curve areas, an increase of the weak acidity percentage from 15% of Silicalite-1 to 22%, 25% and 31% for B-MFI, Fe-MFI and Al-MFI was respectively found.

Table 1 Textural properties of MFI-type samples

Sample	Si/T_{bulk} [a]	$S.A._{BET}$ [b] ($m^2\ g^{-1}$)	$Area_{exter}$ [c] ($m^2\ g^{-1}$)	$V_{micropor.}$ [c] ($cm^3\ g^{-1}$)	d_{pore} (Å)
Silicalite-1	∞	408	345	0.110	33
B-MFI	95	366	195	0.087	23
Fe-MFI	100	406	204	0.094	29
Al-MFI	100	405	233	0.079	32

[a] Measured by A.A. [b] Calculated using the BET method. [c] Calculated using the *t*-plot method.

The nature of acid sites present in Silicalite-1, B-MFI, Fe-MFI and Al-MFI was investigated by FT-IR adsorption of pyridine, having a steric encumbrance similar to the molecules involved in the etherification reaction.[30,31] Fig. 3 shows the infrared spectra in the range of 1700–1400 cm^{-1}, commonly used to identify Lewis and Brønsted acid sites, of a representative sample (Al-MFI), where the red line indicates the spectrum obtained after adsorption of pyridine, and black and green lines refer to the profiles after outgassing at room temperature and 150 °C, respectively.

Table 2 reports the concentration of the Lewis and Brønsted acid sites of the catalysts, obtained after deconvolution of the peaks at 1445 cm^{-1} and 1545 cm^{-1}, respectively.[31,32] Silicalite-1 presents the lowest acidity with a major contribution of Lewis acid sites and a very low content of strong Brønsted acid sites (9 μmol g_{cat}^{-1}). As expected and according to TPD results, the modification of Silicalite-1 structure with B, Fe and Al increases the acidity of Silicalite-1 and introduces both Lewis and Brønsted acid sites. The Al-MFI catalyst presents the highest acidity, with a major contribution of weak Lewis sites (307.7 μmol g_{cat}^{-1}) and a concentration of strong Brønsted acid sites of 56.6 μmol g_{cat}^{-1}.

Catalytic activity and reaction network

The catalytic performance of the samples was studied in the etherification of HMF, using ethanol as the reactant and solvent, at 140 °C and autogenous pressure. Fig. 4 reports the time course of HMF conversion for all synthesized catalysts. All catalysts were active in the etherification reaction of HMF showing a similar trend with an increase of HMF conversion during the reaction time until reaching a plateau after 5 hours. The catalytic activity of the samples follows the total acidity trend, obtaining a higher HMF conversion by using the Al-MFI catalyst, which reaches 91% at the end of the reaction.

Table 3 reports the pseudo-first order rate constants for HMF depletion, which can be estimated from the data reported in Fig. 4 and the turnover frequencies determined with respect to the overall amount of Lewis and Brønsted sites, as determined by FT-IR measurements (Table 2).

The pseudo-first-order rate constant for the HMF overall conversion increases in going from Silicalite-1 to Al-MFI, in agreement with the conversion data (Fig. 4). If the turnover frequency is analyzed with respect to the amount of acid sites determined by pyridine adsorption, it could be observed that the turnover frequency is essentially independent on the heteroatom when considering the sum of strong Lewis and Brønsted acid sites. An expected maximum in the turnover frequency for the B-MFI sample is observed due to the minor content of strong Lewis acid sites (see Table 2).

In this series of catalysts, both strong Lewis and Brønsted acid sites are active in HMF conversion. The behaviour is determined from the amount of strong acid sites, which is influenced by the introduction of heteroatoms. These findings are also confirmed by the direct correlation observed between the acid site density and the rate constant of HMF conversion (Fig. 5). Also in this case, a deviation was observed for B-MFI which presents the lowest acid site density.

The reaction products, 5-(ethoxymethyl)furan-2-carbaldehyde (EMF), ethyl 4-oxopentanoate (EOP),

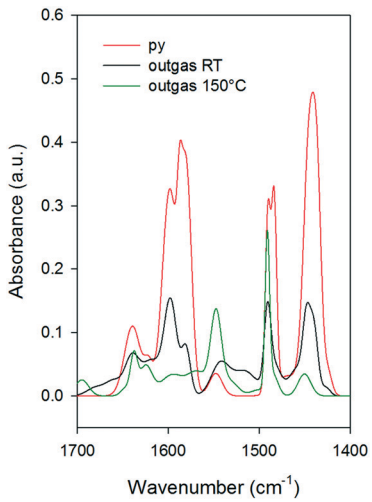

Fig. 3 FT-IR spectra of the Al-MFI sample in the 1700–1400 cm^{-1} region after adsorption of pyridine (red line) and evacuation at room temperature (black line) and at 150 °C (green line).

Table 2 Brønsted and Lewis acid sites distribution of the catalysts obtained from pyridine FT-IR measurements

	Lewis acid sites (μmol g_{cat}^{-1})		Brønsted acid sites (μmol g_{cat}^{-1})
Sample	Weak[a]	Strong[b]	Strong[c]
Silicalite-1	30.4	20.7	9.0
B-MFI	124.4	10.8	13.4
Fe-MFI	122.3	23.3	35.4
Al-MFI	307.7	31.1	56.6

[a] Calculated using the band at 1445 cm^{-1}, r.t. [b] Calculated using the band at 1445 cm^{-1}, 150 °C. [c] Calculated using the band at 1545 cm^{-1}, 150 °C.

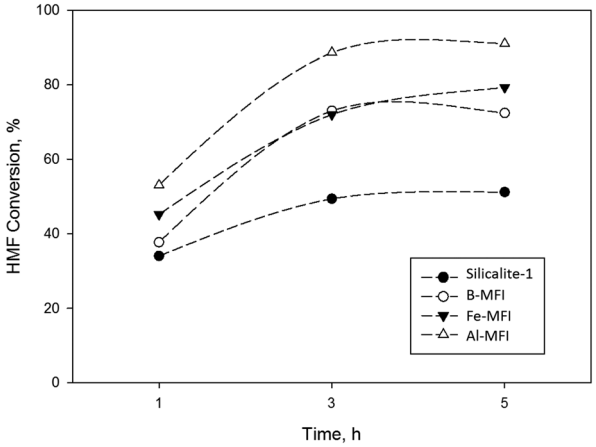

Fig. 4 Time course of HMF conversion for all synthesized catalysts.

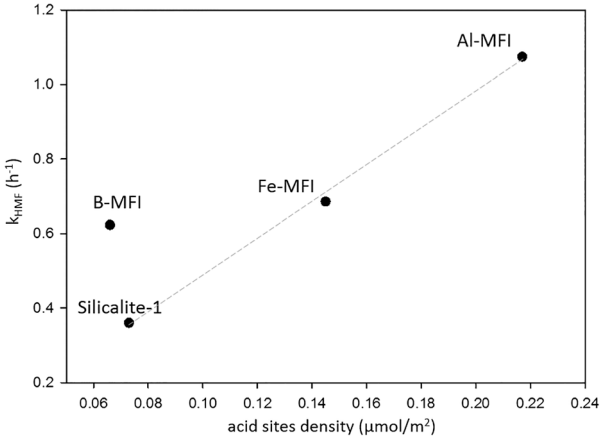

Fig. 5 Trend of the rate constant of HMF depletion with the acid sites density.

5-(hydroxymethyl)furfural diethyl acetal (HMFDEA) and 5-(ethoxymethyl)furfural diethyl acetal (EMFDEA), were identified and quantified by GC-FID analyses in the final solution (Scheme 1). The direct etherification of the hydroxyl group of HMF leads to the formation of EMF, whilst EOP is obtained by the opening of the furanic ring.

In previous studies,[4b,33] we revealed two main conversion pathways for HMF, leading to the formation of EMF and EOP, activated by the different nature of acidic sites. A secondary route for the formation of EOP starting from EMF was furthermore proposed.[4a] In the present work, it was possible to identify the formation of acetals, HMFDEA obtained by acetalization of HMF and EMFDEA formed through etherification of the free hydroxyl functional group of HMFDEA.

Fig. 6 shows the product distribution for each catalyst as a function of reaction time. For the Silicalite-1 catalyst, the yield of EMF, the main reaction product, increases with time and reaches its maximum value after 5 hours of reaction.

A second aspect to be highlighted is the high yield of HMFDEA at the lowest conversion values in the first hour of reaction.

Moreover, the highest value of EMFDEA yield is observed at the third hour of reaction with a subsequent drop when increasing the reaction time. The yield of EOP always remains below 2%, in accord with the low Brønsted acidity of this catalyst.

Table 3 Pseudo-first order rate constants and turnover frequencies for HMF depletions

Sample	Rate constant, k_{HMF} (h^{-1})	Turnover frequency[a] (h^{-1} μmol^{-1})
Silicalite-1	0.360	0.121
B-MFI	0.623	0.257
Fe-MFI	0.685	0.117
Al-MFI	1.074	0.122

[a] Rate constant (h^{-1}) divided by the amount of strong Lewis and Brønsted sites (μmol) determined by FT-IR pyridine measurements.

The increase of the catalyst acidity due to the introduction of different heteroatoms in the Silicalite-1 structure favours the formation of EMF. For the Al-MFI catalyst, which presents the major quantity of Lewis acid sites, an EMF yield of 70% is observed after five hours of reaction. Moreover, it is possible to prove that the increase of the acidity also affects the pathway to HMFDEA, which shows the highest yields during the first hour of reaction and then decreases faster than in the case of Silicalite-1 catalyst. The distribution of the reaction products during the course of the etherification reaction allows us to hypothesize two different routes of HMF etherification, *i.e.* direct etherification and a parallel pathway *via* acetalization.

In order to confirm this hypothesis, specific tests starting from an ethanolic solution of HMFDEA were carried out under the same experimental conditions. Fig. 7 shows that almost 90% of HMFDEA is consumed during the first hour of reaction, leading to the formation of EMFDEA, EMF and EOP. Between 1 and 5 h, a complete conversion of HMFDEA and EMFDEA is observed, yielding EMF as the main product.

At the end of all the reactions, the mass balance is always about 90%; the missing 10% is due to the formation of humins and other condensed products (see Table S1 in the

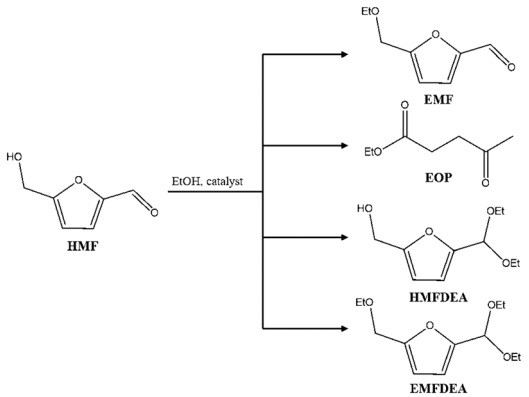

Scheme 1 Reaction products of HMF etherification.

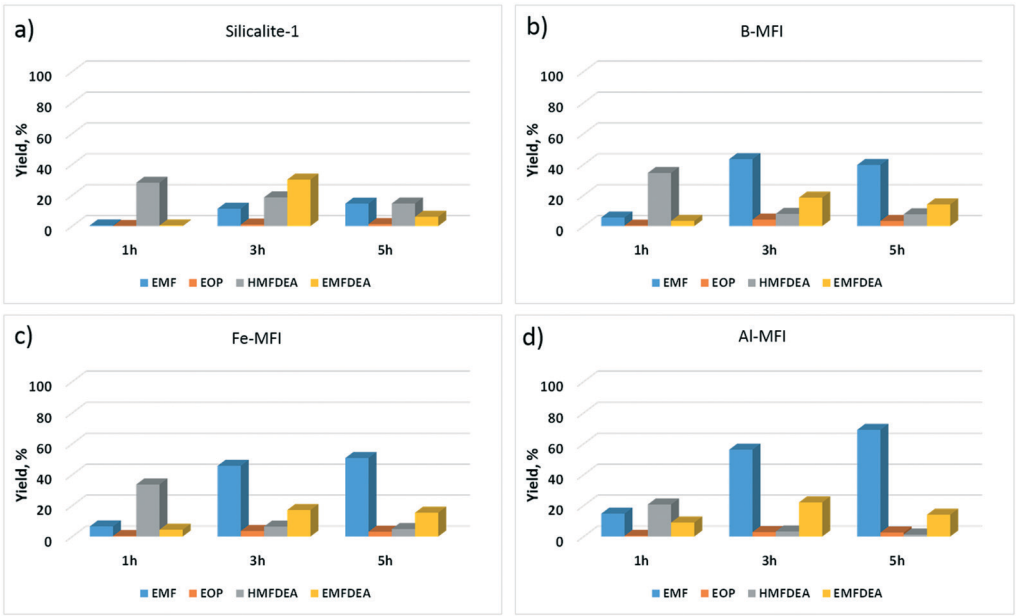

Fig. 6 Evolution of product yields for the catalysts Silicalite-1 (a), B-MFI (b), Fe-MFI (c) and Al-MFI (d).

ESI†). The results discussed above are in accordance with the reaction scheme presented in Scheme 2, in which a pathway of EMF formation *via* acetals is evidenced, with two different equilibria between HMF ↔ HMFDEA and EMF ↔ EMFDEA. The proposed reaction pathway is also in agreement with the results of Lewis *et al.*[34]

The reaction system was modelled as an isotherm–isochoric uniformly mixed batch reactor, assuming a first-order kinetic equation for all reaction steps, after verification that this simplified model provides a reasonably good description of the catalytic behavior. Due to the large excess of ethanol, the concentration of the alcohol was assumed constant and not considered in the kinetic equation.

The following material balances can be written:

$$\frac{1}{V}\cdot\frac{dn_{HMF}}{dt} = -k_1\cdot C_{HMF} - k_2\cdot C_{HMF} + k_{2r}\cdot C_{HMFDEA} \quad (1)$$

$$\frac{1}{V}\cdot\frac{dn_{HMFDEA}}{dt} = k_2\cdot C_{HMF} - k_{2r}\cdot C_{HMFDEA} - k_3\cdot C_{HMFDEA} \quad (2)$$

$$\frac{1}{V}\cdot\frac{dn_{EMFDEA}}{dt} = k_3\cdot C_{HMFDEA} - k_4\cdot C_{EMFDEA} + k_{4r}\cdot C_{EMF} \quad (3)$$

$$\frac{1}{V}\cdot\frac{dn_{EMF}}{dt} = k_1\cdot C_{HMF} + k_4\cdot C_{EMFDEA} - k_{4r}\cdot C_{EMF} - k_5\cdot C_{EMF} \quad (4)$$

$$\frac{1}{V}\cdot\frac{dn_{EOP}}{dt} = k_5\cdot C_{EMF} \quad (5)$$

where n_i and C_i are the mole number (mmol) and molar concentration (mmol l^{-1}) of i-th species, respectively, whilst V is the reaction volume fixed at 3.5 ml and t is the reaction time (h).

The absence of mass transfer limitations verified as well that the first-order kinetics correctly describes the behaviour.

Fig. 8 shows the fitting of the experimental data, whilst Fig. 9 compares the model predictions and experimental data to evidence the overall satisfactory correlation.

Table 4 summarizes the estimated rate constants as a function of catalyst composition for all the reaction steps of the reaction network indicated in Scheme 2.

Role of acid sites in various steps of the reaction network

The analysis of the dependence of the rate constants in the reaction network of HMF etherification on the catalyst composition (Table 4), in relation to the quantification of their

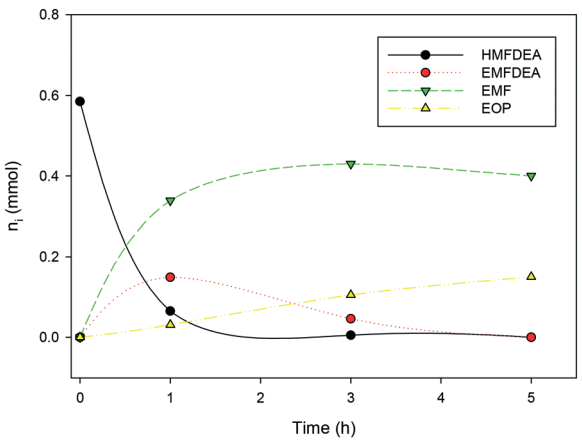

Fig. 7 Evolution of EMFDEA, EMF and EOP products during the etherification of HMFDEA.

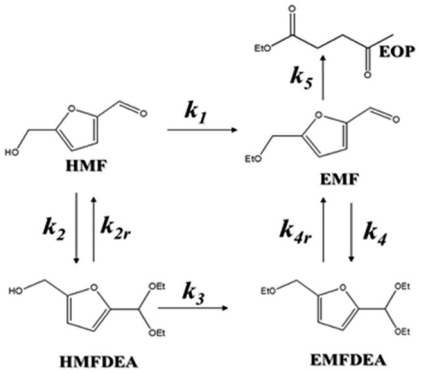

Scheme 2 Proposed reaction network in the etherification of HMF with ethanol.

acidity by FT-IR pyridine adsorption (Table 2), provides some interesting insight into the relationship between the type and amount of acid sites and different reactivities over the proposed reaction scheme.

As mentioned before analysing the turnover frequency of this series of catalysts (Table 3), the HMF conversion is a function of the total amount of Lewis and Brønsted acid sites, rather than the nature of heteroatoms.

This may suggest that the introduction of the heteroatoms in the synthesis changes the amount of acid sites rather than their specific activity. However, this general observation may be not valid if the specific rates in the reaction network are analysed. It is noteworthy that the proposed discussion is based on the acidity measured *via* FT-IR pyridine adsorption data, providing a good quantification of the amount of the different acid sites. The acid site estimation *via* NH_3-TPD measurement are in line with the FT-IR results, although with some differences since i) it is not possible to discriminate between Brønsted and Lewis acid sites in the NH_3-TPD test and ii) ammonia might reach some sites not accessible by pyridine, due to its reduced molecular size. On the other hand, accessibility by pyridine is more representative of the accessibility by HMF.

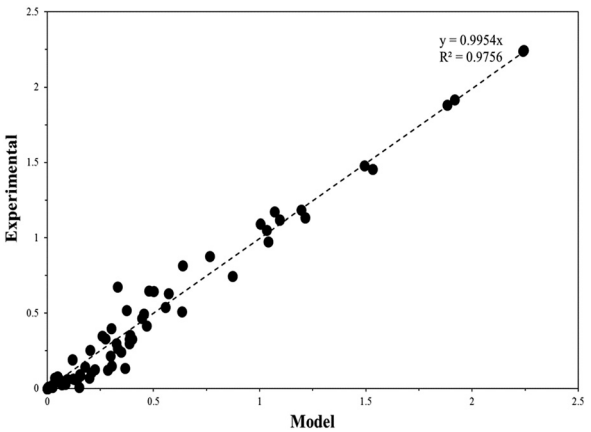

Fig. 8 Comparison between the model (line) and experimental data (symbol).

From the analysis of the k_1 parameter in Table 4, it clearly appears that the presence of aluminum is necessary to promote the direct etherification of HMF to EMF, since only Al-MFI shows a non-zero k_1 value. Although there is no detailed analysis of the reaction network in this paper, previous works showed that this reaction step is catalysed preferably by Lewis acid sites.[4b] Despite the fact that the B and Fe samples also presented some Lewis acidity, no activity towards direct HMF-to-EMF conversion was observed, suggesting that only Lewis acid sites generated from aluminum species could be effective for this reaction step.

On the contrary, if the EMF-to-EOP step is considered, Table 4 shows an inverse correlation, *i.e.* the lower the overall acidity, the higher the rate constant k_5. In a previous work carried out over Silicalite-1 samples,[4b] it was shown that the EMF ring opening to EOP was promoted by strong Brønsted acid sites, whilst the results presented here show an opposite trend. However, this issue could be clarified by considering the different features of Brønsted acid sites. In fact, it is well known that Brønsted acid sites in zeolites commonly refer to both bridging OH groups (SiOH-T, T = B, Fe, Al) and silanol groups. In Silicalite-1, the strong Brønsted sites detected *via* FT-IR analysis can be associated with silanol groups.[4b] Therefore, since Silicalite-1 showed the maximum k_5 value, Si–OH groups could be assumed as the most active towards the EMF-to-EOP reaction step. It should be also noted that the higher activity of Silicalite-1 is related to its higher external surface area (Table 1) where these silanol groups are preferentially located. FT-IR characterization of these samples, not reported here for conciseness, is in good agreement with this interpretation.

If the reversible reaction step HMF ↔ HMFDEA is considered, it was found that the k_2/k_{2r} ratio linearly depends on the Brønsted acid site concentration (Fig. 10), confirming that the acetalization reaction is favoured by the increase of Brønsted acidity.[34] Therefore, also for this step, Al-MFI shows the highest activity, followed by Fe-MFI, B-MFI and Silicalite-1. The conversion of EMFDEA to EMF (deacetalization) is also favoured by the increase of the Brønsted acid site concentration (Fig. 10). Table 5 reports the turnover frequencies estimated for direct HMF acetalization (HMF ↔ HMFDEA) and EMFDEA deacetalization (EMFDEA ↔ EMF) reactions, by considering the k_2/k_{2r} or k_{4r}/k_4 ratio for HMF ↔ HMFDEA or EMFDEA ↔ EMF, respectively, as a measure of the net reaction divided by the amount of strong Brønsted acid sites (determined by FT-IR pyridine adsorption).

We may note that i) the turnover frequencies for Silicalite-1 and B-MFI samples are about twice those for Fe-MFI and Al-MFI samples for both direct acetalization and deacetalization reactions, and ii) the turnover frequency of deacetalization (EMFDEA ↔ EMF step) is at least 4 times higher than that of the direct acetalization step (HMF ↔ HMFDEA). The first aspect indicates that the intrinsic reactivity of the strong Brønsted acid sites in Silicalite-1 and B-MFI is about two times higher than that of Fe-MFI and Al-MFI in the acetalization reaction, contrary to what may be expected.

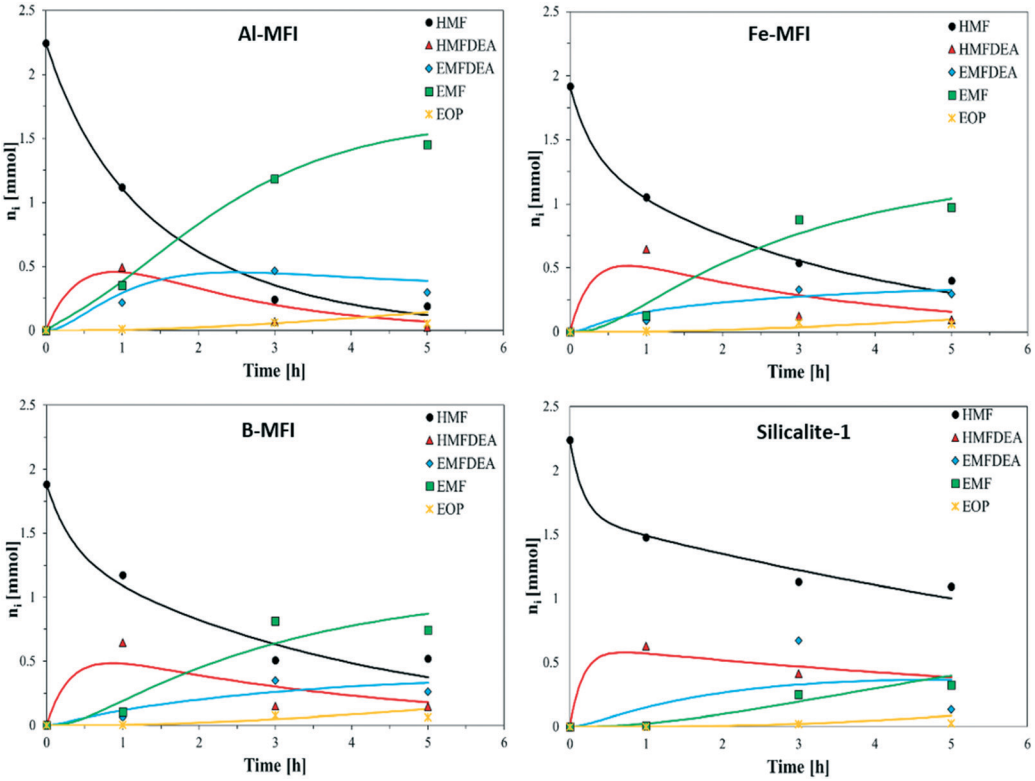

Fig. 9 Comparison between experimental species moles and model predictions.

This is likely related to the preferential presence of strong acid silanol groups associated with surface defects on the external surface[4b] in Silicalite-1 and B-MFI rather than in Fe-MFI and Al-MFI samples, in agreement with the SEM data (Fig. 2) and FT-IR characterization of these samples, which is not reported here for conciseness.

The second aspect may appear rather contradictory. In fact, the same type of strong Brønsted acid sites apparently catalyzes the direct acetalization (HMF ↔ HMFDEA) and the EMFDEA deacetalization (EMFDEA ↔ EMF). While there is a difference in the electron donating character of the ethoxy group in EMF with respect to the hydroxyl group in HMF, it is unlikely that this is the main reason for this effect. However, we should consider that even if not indicated in Schemes 1 and 2, the acetalization reaction leads to the formation of water (Scheme 3) as does the etherification reaction. With the progress of the reaction, the water formed tends to favour the deacetalization reaction, and this explains why with the progress of the reaction the deacetalization (reaction step 4) is favoured over the direct acetalization (reaction step 2).

The results discussed up to now indicate that either Lewis or Brønsted acid sites catalyze the reaction steps in the HMF etherification reaction network. However, we could note that reaction step 3 (HMFDEA to EMFDEA) depends instead on the ratio between strong Brønsted and Lewis acid sites, rather than on their specific amounts.

Table 4 Pseudo-first order rate constants for the reaction steps in the HMF etherification network

Rate constant (h^{-1})	Al-MFI	Fe-MFI	B-MFI	Silicalite-1
k_1	0.172	0	0	0
k_2	0.653	1.200	1.020	1.630
k_{2r}	0.487	1.740	1.590	3.980
k_3	1.190	0.901	0.814	0.357
k_4	0.235	1.070	2.140	0.200
k_{4r}	1.210	3.780	6.010	0.375
k_5	0.030	0.032	0.051	0.106
R^2	0.992	0.980	0.961	0.969

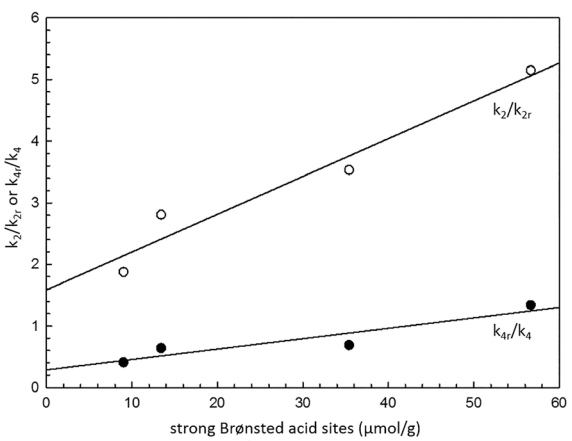

Fig. 10 The effect of Brønsted acid sites concentration on k_2/k_{2r} and k_{4r}/k_4 rate coefficient ratios.

Table 5 Turnover frequency for reversible acetalization reaction steps

	Turnover frequency[a]	
Sample	HMF ⟷ HMFDEA	EMFDEA ⟷ EMF
Silicalite-1	0.46	2.08
B-MFI	0.48	2.10
Fe-MFI	0.19	1.00
Al-MFI	0.24	0.91

[a] k_2/k_{2r} (HMF ⟷ HMFDEA) or k_{4r}/k_4 (EMFDEA ⟷ EMF) divided by the amount of strong Brønsted acid sites (μmol) determined by FT-IR pyridine measurements.

This is evidenced in Fig. 11 which shows that the rate constants of this step k_3 linearly depend on the B/L ratio. A relevant result emerging from the analysis of the rate constants of the various steps (Table 4) is that the HMFDEA etherification (reaction step 3) showed a rate constant about one order of magnitude higher than the direct HMF etherification (reaction step 1).

This could be explained with the different types of coordination. Lewis acid sites catalyse the etherification by non-dissociative adsorption of the hydroxyl group, which as a result becomes a better leaving group.[35] The C═O group in aldehyde, however, can compete with chemisorption, while this competition is inhibited in the acetal. This result thus indicates that, even limited from the reversible reactions of direct HMF acetalization (reaction step 2) and deacetalization of the EMFDEA, the formation of EMF *via* acetal is preferable over the direct route (reaction step 1). However, a fine control of the amount of water in the reaction medium should be necessary to favour first the acetalization (reaction step 2) and then the deacetalization (reaction step 4).

Conclusions

The analysis of the dependence of the rate constants for the various steps in the reaction network of HMF etherification evidences the different roles played by Lewis and Brønsted acid sites and some cooperation effects. The results thus provide new insights into the effect of catalyst properties on HMF conversion.

The strong Lewis acid sites generated from the presence of aluminum are primarily active to catalyze the direct HMF etherification to EMF. If the amount and the strength of Lewis acid sites are not sufficient to promote the direct etherification, the formation of EMF occurs *via* acetalization on Brønsted acid sites. Brønsted acid sites promote acetalization reactions, when H_2O is not present, whilst the deacetalization reaction is favoured in the presence of water, formed from

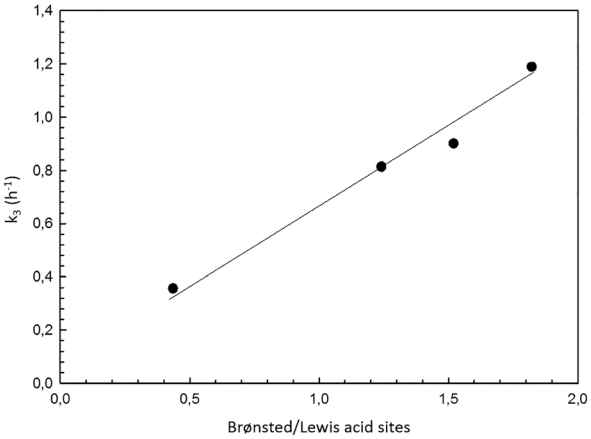

Fig. 11 The effect of strong Brønsted acid site-to-strong Lewis acid site ratio on the k_3 rate coefficient.

both acetalization and etherification reactions. A high Brønsted acid sites concentration is required in order to achieve a fast transformation of acetals into EMF. According to these observations, Al-MFI can be considered as the preferable catalyst among the investigated zeolites, showing the highest HMF conversion, the highest EMF productivity, and the lowest amount of intermediates after 5 h of reaction. The superiority of Al-MFI can be related to the presence of highly active Lewis sites that promote the HMF to EMF reaction and the large amount of Brønsted acid sites that favour the transformation of intermediates into EMF.

The analysis of the turnover frequency provides some further insights. The values of turnover frequency calculated for HMF depletion indicate a simple correlation with the total amount of strong Brønsted and Lewis acid sites without a specific effect of the heteroatoms in changing the strength of the acid sites. Moreover, the analysis of the single reaction steps provides some different observations, in addition to the observation that only the strong Lewis acid sites present in Al-MFI are able to catalyze the direct EMF synthesis from HMF (reaction step 1).

In the direct HMF acetalization (HMF ⟷ HMFDEA, reaction step 2) and EMFDEA deacetalization (EMFDEA ⟷ EMF, reaction step 4) reactions, the turnover frequencies, calculated considering the strong Brønsted acid sites, for Silicalite-1 and B-MFI samples are about twice those for Fe-MFI and Al-MFI samples. This is likely related to the different reactivity of strong silanol groups generated by external surface defects in Silicalite-1 and B-MFI, as confirmed by SEM and FT-IR results. These sites are also responsible for the EMF-to-EOP reaction.

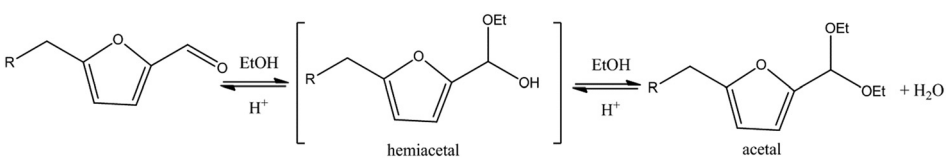

Scheme 3 Formation of acetal.

Finally, the acetal etherification (HMFDEA to EMFDEA, reaction step 3) depends on the ratio between the Brønsted and Lewis acid sites, suggesting that their cooperation in this reaction is different from reaction step 1 (direct etherification), whose rate constants are about one order of magnitude lower with respect to those of the acetal etherification. The etherification proceeds *via* non-dissociative adsorption of the hydroxyl group on Lewis acid sites, making the hydroxyl functionality a better leaving group. However, the aldehyde group in HMF can compete with chemisorption, while this competition is inhibited in the acetal, and as a consequence the HMFDEA to EMFDEA reaction proceeds faster.

Experimental section

Materials

The investigated samples were synthesized by using tetrapropyl ammonium bromide as the structure directing agent (SDA) and by adopting an alkaline synthesis gel with composition reported in Table 6. Precipitated silica (Merck) was used as the silica source for the synthesis of Silicalite-1, B-MFI and Al-MFI whilst fumed silica was used to prepare Fe-MFI. $Al(OH)_3$, $Fe(NO_3)_3{\cdot}9H_2O$ and H_3BO_3 were used as trivalent atom sources for the synthesis of the respective T-MFI-type samples (T = B, Fe, Al). In order to obtain T-MFI-type materials with a similar Si/T ratio in the final solid (about 100), the gel composition was optimized on purpose. The Si/T ratio in the gel was then different, due to the different capacity of boron, iron and aluminum to be incorporated into the MFI framework.

Crystallization was carried out under hydrothermal conditions using a Teflon-lined stainless-steel autoclave kept in a static oven at 170 °C for 24 hours for Silicalite-1 and Fe-MFI. A crystallization period of 72 hours was necessary to synthesize B-MFI and Al-MFI. After crystallization, the solid was recovered by filtration, washed several times with distilled water and dried at 110 °C overnight. A calcination treatment at 550 °C in an air flow for 8 hours (heating rate of 5 °C min^{-1}) was carried out to remove the organic SDA molecules. The protonic form of the catalysts was obtained by double ion-exchange with NH_4Cl (1 M) at 80 °C, followed by calcination under static air conditions at 550 °C for 8 hours.[13]

Catalyst characterization

X-Ray powder diffraction spectroscopy (APD 2000 Pro) was used to evaluate the crystallinity and purity of the synthesized phases.

The Si/T ratio (T = B, Fe or Al) in the solid was measured using an atomic absorption spectrometer GBC 932 AA.

The morphology of the crystalline phase of the samples has been examined using a PhenomProX desktop scanning electron microscope (SEM).

The specific surface area and the micropore volume were estimated by BET and *t*-plot models, respectively, by measuring nitrogen adsorption isotherms at −196 °C using an ASAP 2020 Micromeritics instrument.

NH_3-TPD measurements were conducted using a TPDRO1100 apparatus (ThermoFisher). A dried sample (100 mg, pellet mesh 90–150 μm) was loaded in a tubular quartz micro-reactor and pretreated at 300 °C in helium flow for 1 hour to remove adsorbed water. The sample was then cooled down to 150 °C and saturated with a 10% v/v NH_3/He mixture with a flow rate of 20 STP mL min^{-1} for 2 hours. Physically adsorbed ammonia was removed by purging in helium at 150 °C for 1.5 hours until TCD baseline stabilization. Desorption measurements were carried out in the temperature range of 100–700 °C (10 °C min^{-1}) using a helium carrier (flow rate of 20 STP mL min^{-1}).[13]

The nature of the acid sites was analyzed by the FT-IR pyridine adsorption technique. FT-IR spectra were collected using a Nicolet iS50 FT-IR spectrometer (resolution 4 cm^{-1}) by means of OMNIC software. All the samples were finely ground in a mortar and pressed in self-supporting wafers. Before IR analysis, all samples were activated under vacuum (10^{-4} Torr) for 1 hour at 400 °C in order to desorb any possible physisorbed species in an IR cell allowing *in situ* thermal treatments and pyridine dosage. The desorption procedure of pyridine was monitored in a stepwise manner by evacuating the sample at room temperature (r.t.) and 150 °C and cooling down after each step to record the corresponding spectrum. The quantification of Lewis and Brønsted strong acid sites was performed by integrating the area underneath the bands at 1445 and 1545 cm^{-1}, using 2.2 cm μmol^{-1} and 1.67 cm μmol^{-1} as the integrated molar extinction coefficient (IMEC), respectively.

Catalytic tests

HMF etherification with ethanol has been carried out in a Parr autoclave reactor (Teflon-lined) provided with a Parr 4848 controller, using 2.5 mmol of HMF, 100 mg of catalyst and 3.5 ml of ethanol at 140 °C for 1, 3 and 5 hours under autogenous pressure.[4] The identification of the products was performed using a Finnigan Trace-GC-FID equipped with an Rxi-5 ms capillary column (length 30 m, diameter 0.25 mm

Table 6 Synthesis conditions for MFI-type zeolites

	Synthesis		
Sample	Molar gel composition	*T* (°C)	*t* (h)
Silicalite-1	$0.08Na_2O$–0.08TPABr–$1SiO_2$–$20H_2O$	170	24
B-MFI	$0.14Na_2O$–0.08TPABr–$1SiO_2$–$0.033H_3BO_3$–$25H_2O$	170	72
Fe-MFI	$0.14Na_2O$–0.08TPABr–$1SiO_2$–$0.005Fe_2O_3$–$0.015H_3PO_4$–$30H_2O$	170	24
Al-MFI	$0.12Na_2O$–0.08TPABr–$0.0042Al_2O_3$–$1SiO_2$–$20H_2O$	170	72

and film thickness 0.25 μm) using pure compounds for the calibration curves. 5-Hydroxymethyl furfural (HMF), 5-(ethoxymethyl)furan-2-carbaldehyde (EMF) and ethyl 4-oxopentanoate (EOP) were purchased from Sigma Aldrich, while acetal compounds were synthesized and purified according to methods described by Balakrishnan *et al.*[3b] and used as standards for the quantification.

The absence of mass and heat transfer limitations during experiments have been verified with conventional tests and estimations.

The carbon balance during catalytic tests was typically good (over 90%), the difference to 100% being due to the formation of some humins and products of condensation, which become relevant only at longer reaction times.

Model parameters were estimated by using the fourth order Runge–Kutta method (MATLAB R2012a) to solve the above differential equation set, coupled with the Levenberg–Marquardt algorithm for non-linear regression analysis. A 95% confidence interval was adopted during the analysis.

Conflicts of interest

There are no conflicts to declare.

Notes and references

1 H. Li, S. Yang, A. Riisager, A. Pandey, R. S. Sangwan, S. Saravanamurugan and R. Luque, *Green Chem.*, 2016, **18**, 5701.
2 M. J. Climent, A. Corma and S. Iborra, *Green Chem.*, 2014, **16**, 516.
3 (*a*) E. R. Sacia, M. Balakrishnan and A. T. Bell, *J. Catal.*, 2014, **313**, 70; (*b*) M. Balakrishnan, E. R. Sacia and A. T. Bell, *Green Chem.*, 2012, **14**, 1626.
4 (*a*) K. Barbera, P. Lanzafame, A. Pistone, S. Millesi, G. Malandrino, A. Gulino, S. Perathoner and G. Centi, *J. Catal.*, 2015, **323**, 19; (*b*) P. Lanzafame, K. Barbera, S. Perathoner, G. Centi, A. Aloise, M. Migliori, A. Macario, J. B. Nagy and G. Giordano, *J. Catal.*, 2015, **330**, 558.
5 E. Salminen, N. Kumar, P. Virtanen, M. Tenho, P. Maeki-Arvela and J.-P. Mikkola, *Top. Catal.*, 2013, **56**, 765.
6 J. Luo, J. Yu, R. J. Gorte, E. Mahmoud, D. G. Vlachos and M. A. Smith, *Catal. Sci. Technol.*, 2014, **4**, 3074.
7 K. S. Arias, M. J. Climent, A. Corma and S. Iborra, *Energy Environ. Sci.*, 2015, **8**, 317.
8 O. Casanova, S. Iborra and A. Corma, *J. Catal.*, 2010, **275**, 236.
9 K. S. Arias, M. J. Climent, A. Corma and S. Iborra, *ChemSusChem*, 2014, **7**, 210.
10 C. J. A. Mota and B. P. Pinto, *Curr. Phys. Chem.*, 2012, **2**, 211.
11 O. D. Bozkurt, F. M. Tunc, N. Baglar, S. Celebi, I. D. Gunbas and A. Uzun, *Fuel Process. Technol.*, 2015, **138**, 780.
12 G. Bozga, I. T. Apan and R. E. Bozga, *Recent Pat. Catal.*, 2013, **2**, 68.
13 E. Catizzone, A. Aloise, M. Migliori and G. Giordano, *Microporous Mesoporous Mater.*, 2017, **243**, 102.
14 E. Catizzone, A. Aloise, M. Migliori and G. Giordano, *Appl. Catal., A*, 2015, **502**, 215.
15 J. G. Goodwin Jr, S. Natesakhawat, A. A. Nikolopoulos and S. Y. Kim, *Catal. Rev.: Sci. Eng.*, 2002, **44**, 287.
16 K. S. Arias, S. I. Al-Resayes, M. J. Climent, A. Corma and S. Iborra, *ChemSusChem*, 2013, **6**, 123.
17 (*a*) R. J. van Putten, J. C. van der Waal, E. de Jong, C. B. Rasrendra, H. J. Heeres and J. G. de Vries, *Chem. Rev.*, 2013, **113**, 1499; (*b*) J. N. Chheda, G. W. Huber and J. A. Dumesic, *Angew. Chem., Int. Ed.*, 2007, **46**, 7164.
18 H. Wang, Y. Wang, T. Deng, C. Chen, Y. Zhu and X. Hou, *Catal. Commun.*, 2015, **59**, 127.
19 M. M. Antunes, S. Lima, A. Fernandes, A. L. Magalhaes, S. Neves, C. M. Silva, M. F. Ribeiro, D. Chadwick, K. Hellgardt, M. Pillinger and A. A. Valente, *ChemCatChem*, 2017, **9**, 2747.
20 (*a*) K. Barbera, P. Lanzafame, S. Perathoner, G. Centi, M. Migliori, A. Aloise and G. Giordano, *New J. Chem.*, 2016, **40**, 4300; (*b*) P. Lanzafame, K. Barbera, G. Papanikolaou, K. Barbera, S. Perathoner, G. Centi, M. Migliori, A. Aloise and G. Giordano, *Catal. Today*, 2018, **304**, 97–102; (*c*) P. Frontera, A. Macario, A. Aloise, P. L. Antonucci, G. Giordano and J. B. Nagy, *Catal. Today*, 2013, **218–219**, 18–29.
21 (*a*) G. Li, E. A. Pidko and E. J. M. Hensen, *Catal. Sci. Technol.*, 2014, **4**, 2241; (*b*) G. Li, E. A. Pidko and E. J. M. Hensen, *ACS Catal.*, 2016, **6**, 4162.
22 H. Li, J. He, A. Riisager, S. Saravanamurugan, B. Song and S. Yang, *ACS Catal.*, 2016, **6**, 7722.
23 J. Dijkmans, M. Dusselier, D. Gabriels, K. Houthoofd, P. C. M. M. Magusin, S. Huang, Y. Pontikes, M. Trekels, A. Vantomme, L. Giebeler, S. Oswald and B. F. Sels, *ACS Catal.*, 2015, **5**, 928.
24 Z. Wang, L. Wang, Y. Jiang, M. Hunger and J. Huang, *ACS Catal.*, 2014, **4**, 1144.
25 (*a*) T. A. J. Hardenberg, L. Mertens, P. Mesman, H. C. Muller and C. P. Nicolaides, *Zeolites*, 1992, **12**, 685; (*b*) F. Feng and K. J. Balkus Jr, *Microporous Mesoporous Mater.*, 2004, **69**, 85.
26 A. Zecchina, S. Bordiga, G. Spoto and L. Marchese, *J. Phys. Chem.*, 1992, **96**, 4985.
27 S. Mintova and V. Valtchev, *Microporous Mesoporous Mater.*, 2002, **55**, 171.
28 (*a*) M. Migliori, A. Aloise and G. Giordano, *Catal. Today*, 2014, **227**, 138; (*b*) R. Srivastava, N. Iwasa, S. Fujita and M. Arai, *Chem. – Eur. J.*, 2008, **14**, 9507.
29 G. Centi, S. Perathoner, F. Pino, R. Arrigo, G. Giordano, A. Katovic and V. Pedulà, *Catal. Today*, 2005, **110**, 211.
30 M. I. Zaki, M. A. Hasan, F. A. Al-Sagheer and L. Pasupulety, *Colloids Surf., A*, 2001, **190**, 261.
31 R. Buzzoni, S. Bordiga, G. Ricchiardi, C. Lamberti, A. Zecchina and G. Bellussi, *Langmuir*, 1996, **12**, 930.
32 C. A. Emeis, *J. Catal.*, 1993, **141**, 347.
33 P. Lanzafame, D. M. Temi, S. Perathoner, G. Centi, A. Macario, A. Aloise and G. Giordano, *Catal. Today*, 2011, **175**, 435.
34 J. D. Lewis, S. Van de Vyver, A. J. Crisci, W. R. Gunther, V. K. Michaelis, R. G. Griffin and Y. Román-Leshkov, *ChemSusChem*, 2014, **7**, 2255.
35 M. Calatayud, A. M. Ruppert and B. M. Weckhuysen, *Chem. – Eur. J.*, 2009, **15**, 10864.

